NUCLEAR INSTRUMENTS AND METHODS 154 (1978) 127-149 ; © NORTH-HOLLAND PUBLISHING CO.

THE DOUBLE FOCUSING IRON-CORE ELECTRON-SPECTROMETER "BILL" FOR HIGH RESOLUTION (n, e⁻) MEASUREMENTS AT THE HIGH FLUX REACTOR IN GRENOBLE

W. MAMPE, K. SCHRECKENBACH, P. JEUCH, B. P. K. MAIER, F. BRAUMANDL, J. LARYSZ and T. von EGIDY*

Institut Laue-Langevin, 38042 Grenoble Cédex, France

Received 16 December 1977

A new high resolution iron-core electron spectrometer (BILL) has been constructed at the High Flux Reactor in Grenoble. It is currently being used for measurements of conversion electrons after thermal neutron capture. An internal target (maximal size 40 cm^2) is irradiated in a thermal neutron flux of 3×10^{14} n cm^{-2} sec^{-1}. The electrons pass through a vertical beam tube, 14 m long and 10 cm in diameter, defining the solid angle of $3.4\times10^{-6}/4\pi$. The spectrometer itself consists of two independent flat electromagnets. Both magnets act as double focusing spectrometers, where the double focusing is achieved by the combination of homogeneous and $1/r$ fields. The first, a 58° deflecting magnet, forms a 10:1 scaled down intermediate image of the large, 14 m distant target in the reactor hall. The dispersion of this magnet is 94 cm. The second magnet views this reduced image with a very high dispersion of 540 cm. The radius of the optic circle of both magnets is 50 cm. The energy range of the spectrometer is 15 keV $< E <$ 10 000 keV. Multi-wire proportional counters are used as detectors. The best measured momentum resolution has been 8×10^{-5} at 300 keV with a target of 2×100 mm^2. Routine measurements have been carried out with targets of 30×100 mm^2 achieving a resolution of $\Delta p/p = 4\times10^{-4}$. The momentum precision of the instrument is 1 part in 10^5 and the sensitivity for neutron capture conversion electrons 300 μb at 400 keV.

1. Introduction

The detailed knowledge of level schemes provides essential insight into nuclear structure. One of the most instructive methods in nuclear spectroscopy is the investigation of conversion electrons and gamma radiation after thermal neutron capture. With this method, nuclei with a sufficiently high capture cross section are accessible. Since this reaction has a relatively high excitation energy of 5–10 MeV, more levels are populated by it than via beta or alpha decay. Conversion electron measurements offer the possibility, usually in conjunction with gamma ray data, of determining the multipolarities of transitions between nuclear levels. This leads, in most cases, to the assignment of spins and parities of those levels. E0 and strongly converted transitions are observable only with conversion electrons.

There exist as well various problems in atomic and solid state physics which can be illuminated by very precise measurements of conversion electron energies and intensities. To study this broad variety of questions, many different types of beta spectrometers, with steadily improving performances, have been developed during the last 30 years[1,2]), but all these instruments could be used mainly for isotopes with neutron cross sections larger than 50 b. Furthermore some of the most precise instruments were constructed for the study of radioactive isotopes.

* Also at Technical University, Munich, Germany.

2. Concept of a high resolution beta spectrometer at a high flux reactor

The electron spectrometer installed at the Research Reactor Munich[3,6]), worked very successfully for 14 years with an average momentum resolution of $\Delta p/p = 2\times10^{-3}$ but with limited sensitivity. Therefore, it was decided to continue the Munich work with an improved spectrometer to be located at the High Flux Reactor in Grenoble. Calculations for the new instrument and first designs were made by H. F. Mahlein[4]). The essential criteria for this electron spectrometer were the following:

a) isotopes with neutron capture cross-sections greater than 1 barn should be accessible to measurement,
b) it should be possible to investigate electron energies up to 10 MeV,
c) the energy precision should be of the order of 10^{-5},
d) the momentum resolution should be better than 5×10^{-4}.

These criteria fixed the spectrometer type in Grenoble. The combination of extremely high sen-

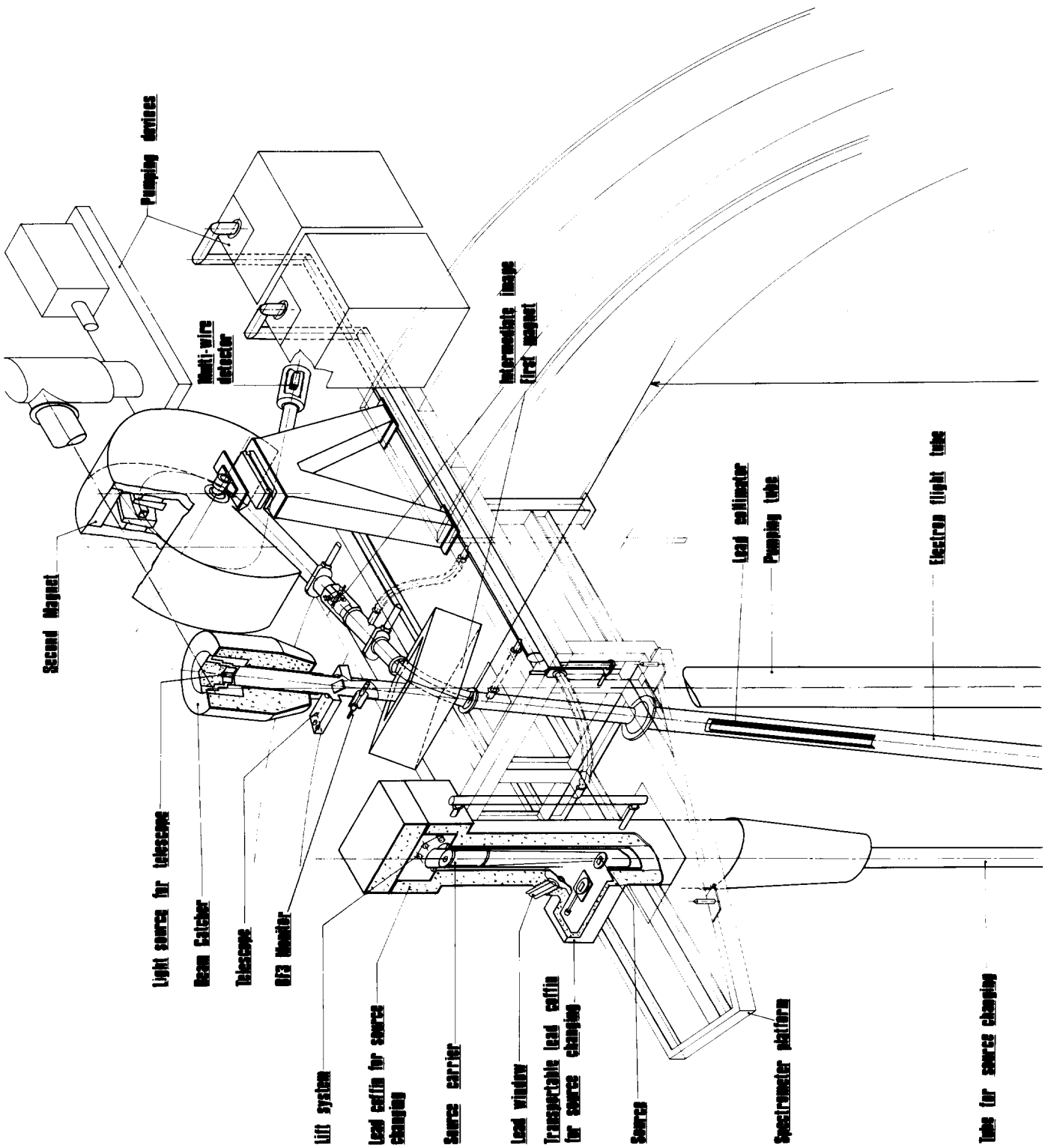
Pumping devices
Multi-wire detector
Intermediate image first magnet
Second Magnet
Lead collimator
Pumping tube
Electron flight tube
Light source for telescope
Beam Catcher
Telescope
Off Monitor
Lift system
Lead coffin for source changing
Source carrier
Lead window
Transportable lead coffin for source changing
Source
Spectrometer platform
Tube for source changing

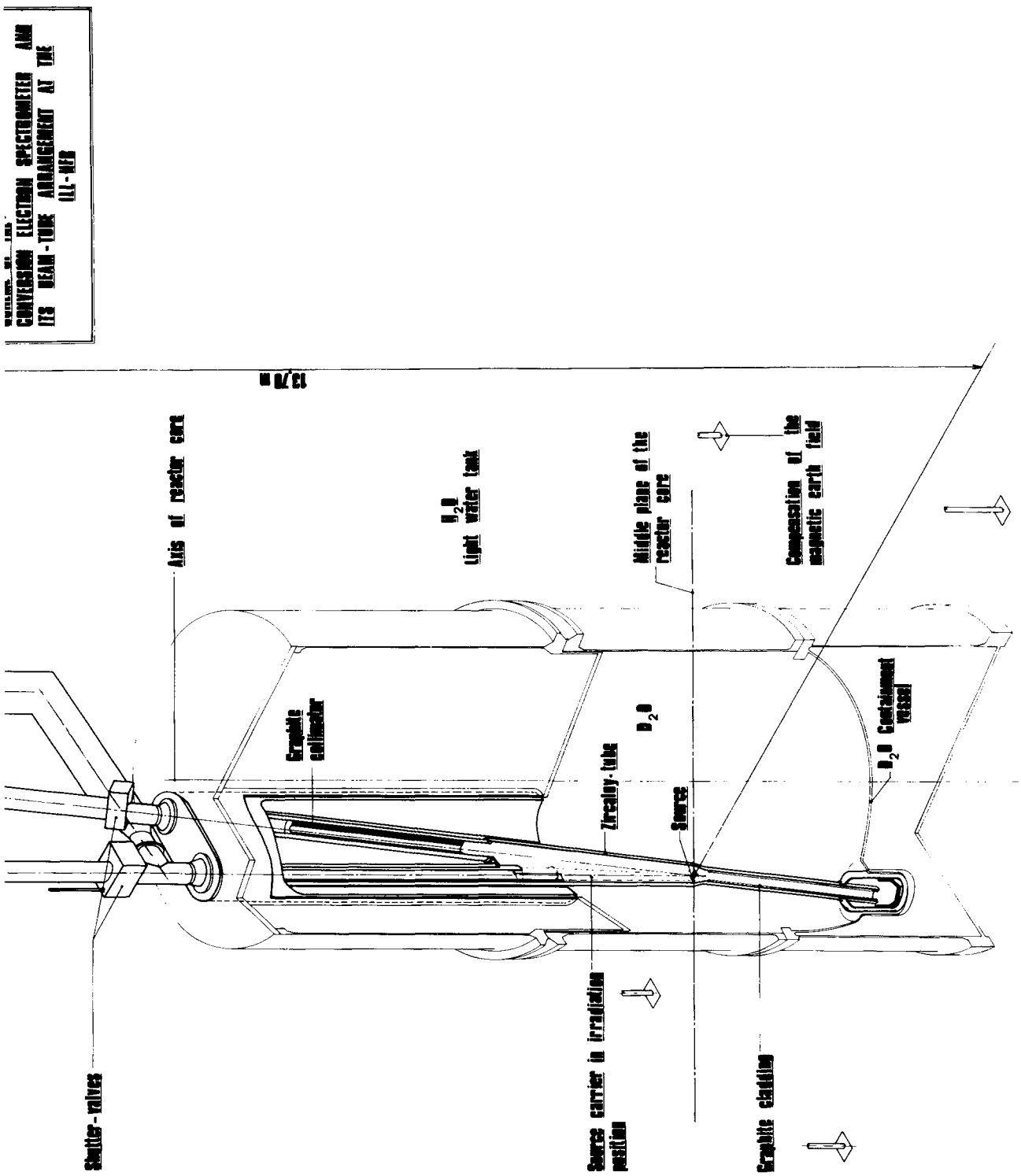

Fig. 1. General view of the spectrometer BILL and the vertical beam tube installed in the reactor.

sitivity and resolution could only be fulfilled by an internal target arrangement. This would allow the use of large targets in a high neutron flux. To obtain high sensitivity, a low background is necessary. Therefore a flat spectrometer, which allows separation of the electrons from the direct beam, was chosen. A consequence of the internal target geometry and the demand for high resolution was the separation of the spectrometer into two independent magnets. The first, an asymmetric magnet, would produce a small image of the remote target. This magnet has only a relatively small deflection angle and, therefore, a small dispersion. The second magnet has the task of producing the high resolving power by means of a high dispersion. An iron-core magnet consisting of homogeneous and $1/r$ fields, satisfies the demands for both double focusing and maximal dispersion. The possibility of adjustment of the fringing fields, necessary for obtaining optimal resolution, was also given by this simple magnet geometry.

An iron free version of the spectrometer was excluded because with such an arrangement it would be impossible to shield the external magnetic fields in a reactor hall sufficiently well.

3. Description of the instrument

3.1. General description

A schematic drawing of the entire instrument, including the special beam tube, is shown in fig. 1. Clearly visible is the heavy water tank of the reactor, into which the lower part of the tube is integrated. The vertical tube of the Y-shaped beam arrangement houses the target changing device and ends in a lead beam catcher. The inclined tube leads the electrons to the spectrometer. The spectrometer is installed on a platform above the reactor swimming pool. The two spectrometer magnets, the beam catcher of the inclined tube, the telescope for observation of the target, the detector, and the pumping device are drawn schematically.

3.2. Beam tube and target

The rather complicated, Y-shaped beam tube is a special construction for the beta spectrometer BILL. A detailed technical description is given by J. C. Faudou and B. P. K. Maier[5]). The tube has an overall length of about 17 m. The bottom of the tube is 175 cm below the target position, where the neutron flux is about 300 times less than at the target. The entire 7 m long part of the beam tube surrounded by D_2O is made of zircalloy II, which has a low capture cross section and a beta decay end point energy of only 1.1 MeV. In order to stop these decay beta rays from contributing to the background directly or via scattering at the target, the bottom and the inner walls of the electron beam tube are covered with a 3 mm graphite layer. The upper part of the beam tube, which is not exposed to the high neutron flux, is made of aluminium.

The 7° inclined electron flight tube carries an upper (1 m long) and a lower (1.6 m) lead collimator; the second one is shielded from the intense reactor radiation by an additional graphite collimator (1 m). Mu-metal tubes mounted inside the beam tube shield external magnetic fields.

3.3 Spectrometer magnets

3.3.1. *General description*

A schematic drawing showing the spectrometer with the arrangement of the two magnets is seen in fig. 2. Both magnets could be used independently as double focusing spectrometers. The first magnet is very similar to the spectrometer at Munich[3]). In our arrangement it is used to produce a small image of the large target. This image then serves as an object for the second magnet which views it with a very high resolving power. An obvious advantage of this telescope arrangement is the possibility of putting a slit at the position of the intermediate image, that is between the magnets. Such a slit prevents electrons not coming from the solid angle subtended by the target from reaching the detector. The photograph (fig. 3) gives a general impression of the instrument.

3.3.2. *Results of the calculations*

A calculation of the focusing characteristics of both magnets, using the transfer matrix method, was made by H. F. Mahlein[4]). The axial and radial deflection of the electrons were treated independently, i.e. only linear terms were taken into account. The fringing fields at the sector edges were considered only in a simple way.

The experimental adjustment has superseded this mathematical simplification. For such an adjustment turnable half cylinders at the edge of the homogeneous field sectors allowed the adjustment of the angle between the field boundaries and the beam. The effect of the half cylinders on the double focusing is described in section 3.4.

The arguments for the choice of combined ho-

mogeneous and $1/r$ fields to obtain double focusing are given in section 2. Here we will only emphasize the particular advantages of a $1/r$ sector field. In the first place, a $1/r$ field has a very high dispersion due to its large gradient ($n = -1$). Secondly, a $1/r$ field is strongly axially focusing (parallel beams are focussed to a line after 90°). It is, however, neither focusing nor defocusing in the radial direction. Thirdly, the mechanical realization of a $1/r$ field (conical pole pieces) is relatively simple with an iron magnet.

Radial and axial electron trajectories in the two magnets are shown in fig. 4. The results of calculations for the two magnets are summarized in table 1.

3.3.3. *Construction of the magnets*

Both magnets were manufactured by Oerlikon

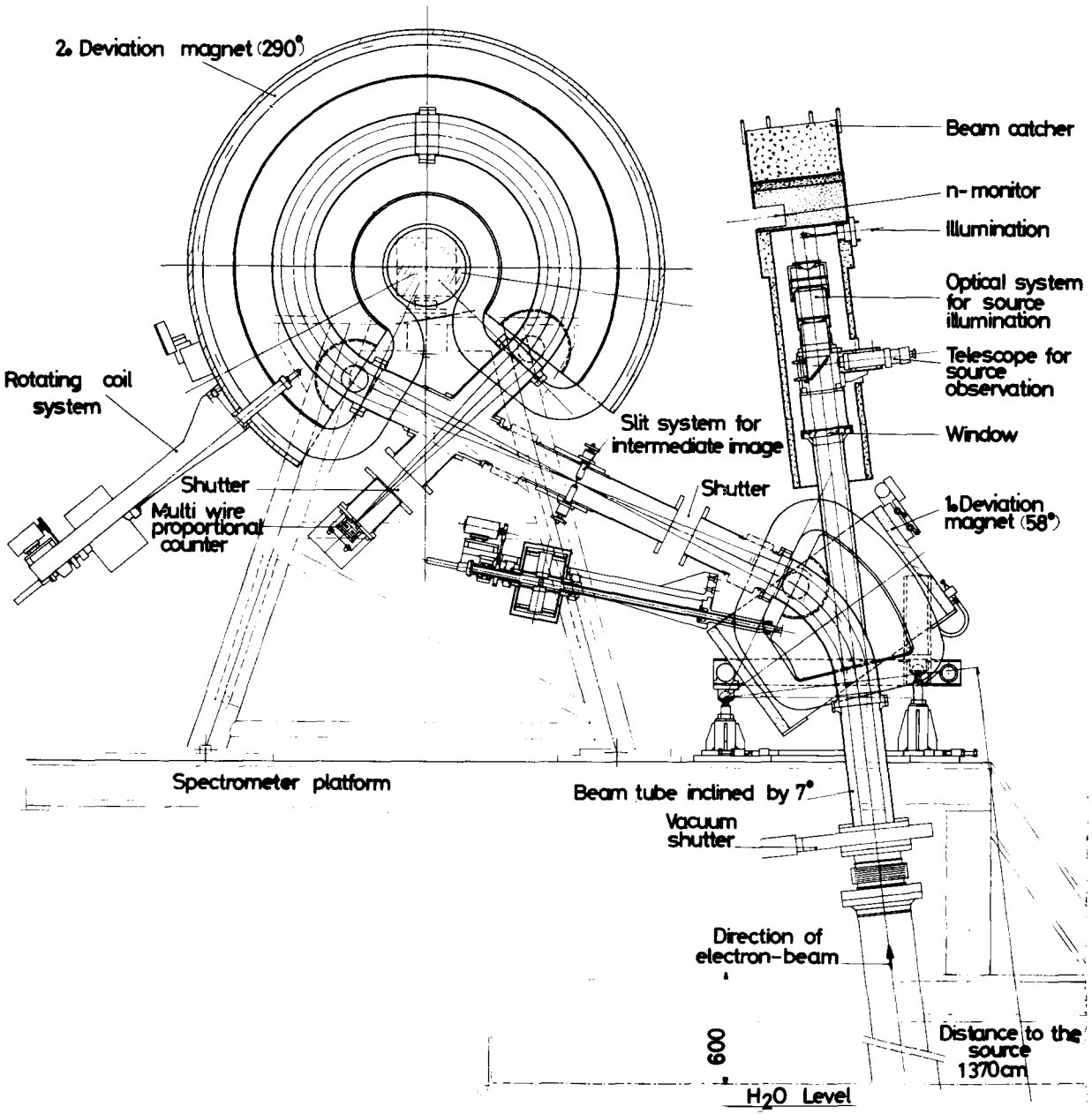

Fig. 2. Schematic view of the spectrometer BILL demonstrating the arrangement of the magnets.

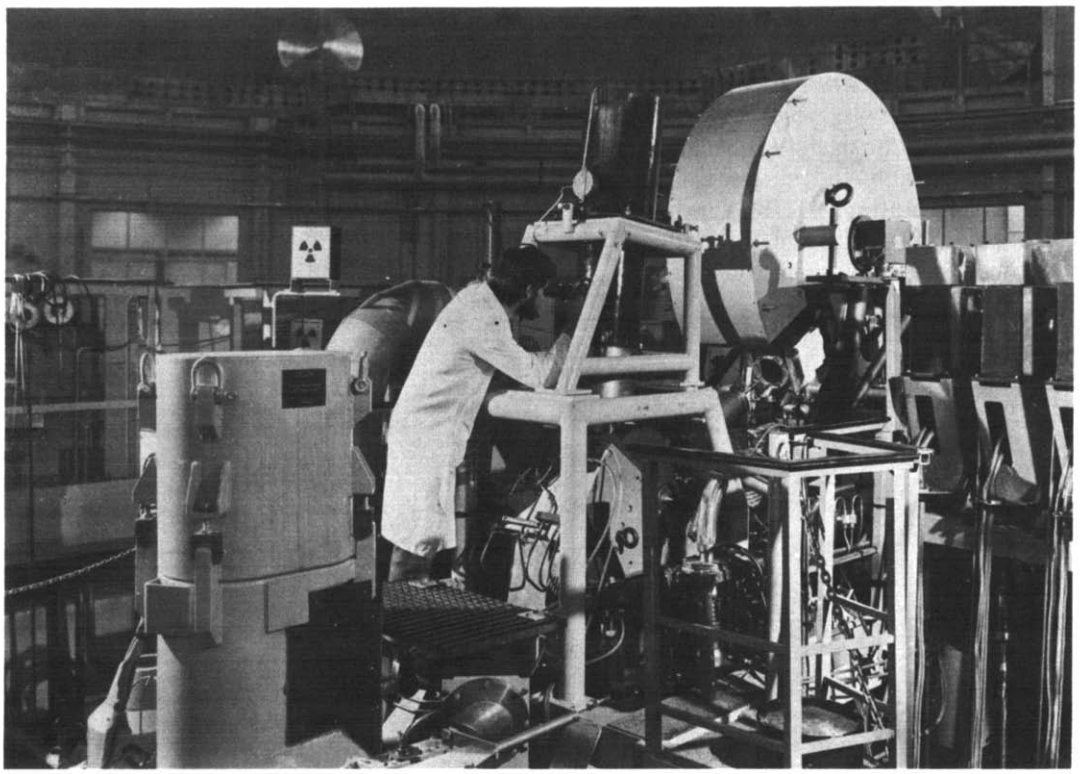

Fig. 3. General view of the spectrometer BILL on the platform above the reactor. From left to right: beam catcher on the target changing tube behind a physicist regarding the target through the telescope, the first magnet in front of the knees of the physicist and the big disk-like second magnet.

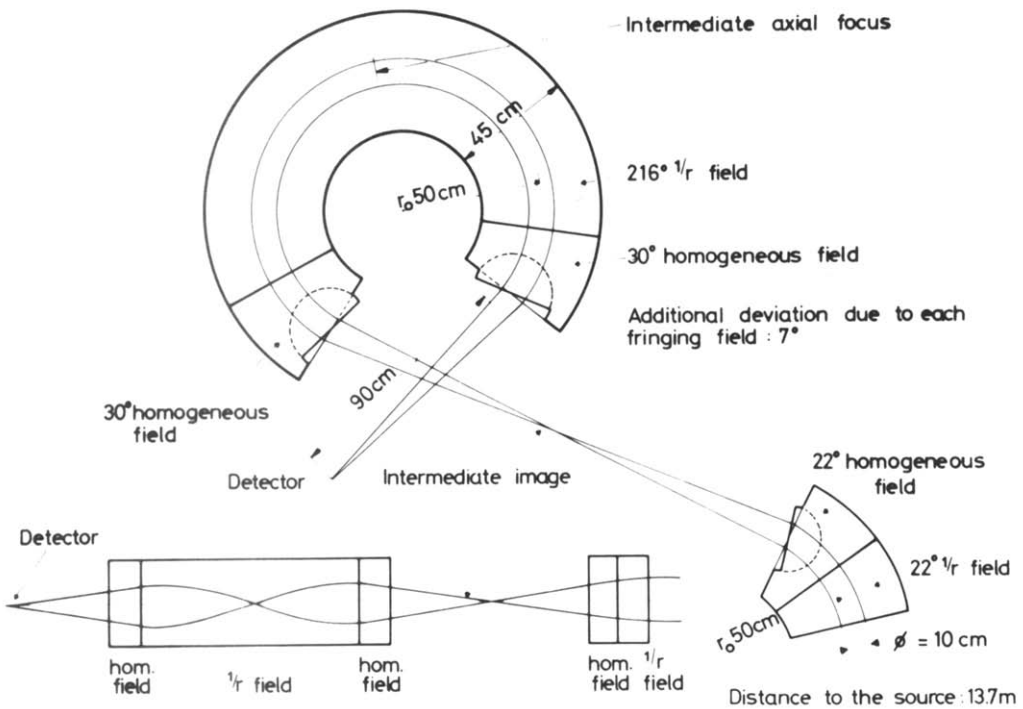

Fig. 4. Radial and axial electron trajectories in the two magnets of BILL.

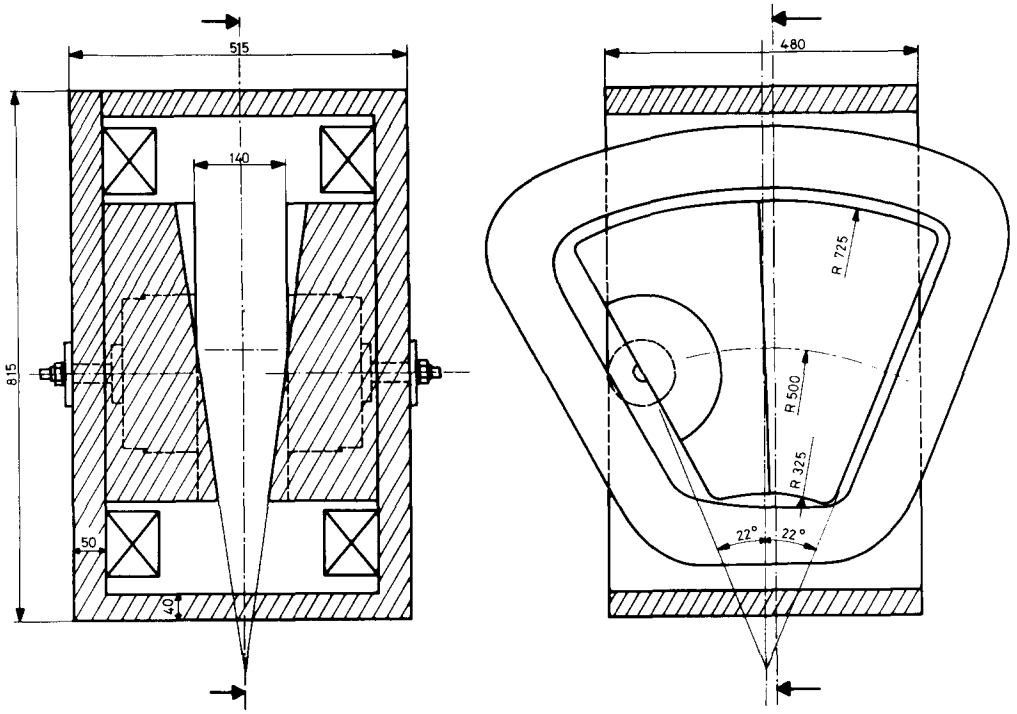

Fig. 5. Dimensions of the 1st magnet of BILL (in mm).

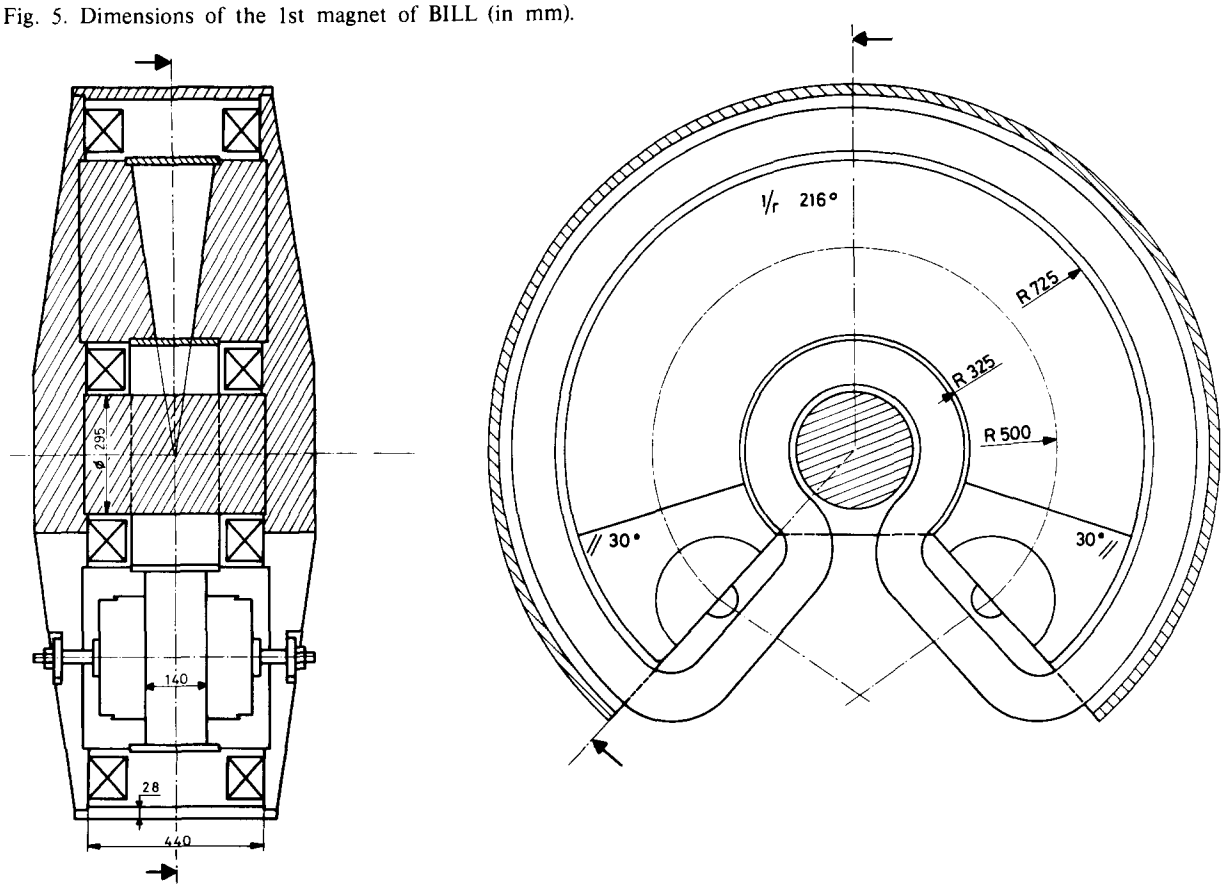

Fig. 6. Dimensions of the 2nd magnet of BILL (in mm).

TABLE 1
Ion optical properties of the two magnets (calculated)[4].

Parameter	1. magnet	2. magnet
Mean radius	50 cm	50 cm
Distance of object	1 370 cm	87 cm
Entrance angle	0	10°
1. homogeneous field	29°	37°
$1/r$-field	29°	216°
2. homogeneous field	none	37°
Total deflecting angle	58°	290°
Exit angle	−5°	10°
Focal length	85.7 cm	87 cm
Radial scaling factor	0.069	−1
Axial scaling factor	0.093	1
Dispersion coefficient	93.8 cm	541.4 cm

(Ornans, France). The dimensions of the first magnet are shown in fig. 5, and for the second in fig. 6. The yoke of the first magnet was made from pure iron (Armco), the yoke of the second magnet, as well as all pole pieces, were constructed from very homogeneous forged soft iron (EN4 Pm 00191a). The magnetization curve of this soft iron is shown in fig. 7. All pieces had undergone a heat-treatment and were tested by the manufacturer using ultra sound of 2 MHz. No anomalies of the homogeneity of the magnetic material were observed (specified to be better than 10^{-3}).

The gap (140 mm) between the pole pieces was made with a precision of ± 0.03 mm. The fields of both magnets were mapped after the delivery with a temperature stabilized Hall probe. This was done at different field settings in order to test the homogeneity of the pole pieces. No field distortions could be detected within the precision of the probe (10^{-4}). The coils of both magnets have 120 turns of 8×8 mm^2 copper wire. The wire has a hole of 4 mm in diameter for water cooling. The resistance of the coils of the first and second magnet are 0.3 Ω and 0.5 Ω, respectively. A current of 40 A produces a gap field of 800 G, which deflects 10 MeV electrons with a mean radius of 50 cm. The vacuum chambers in the magnets are made of aluminium with an elliptic cross section since the maximal radial beam size is larger than the axial size.

3.4. ADJUSTMENT OF THE MAGNETS

Neither the calculations nor the machining or homogeneity of the magnetic material are necessarily of the quality which is required for a high resolution spectrometer. Therefore the optimal characteristics can only be obtained by very careful experimental adjustment. For this adjustment several degrees of freedom were foreseen: variation of the entrance and exit angles of the magnets by turnable half cylinders and variation of the distance of the object (2nd magnet) and the image. In addition, for higher order field corrections shims ought to be used. The adjustment has been done in two steps. Firstly, by recording photographically different trajectories of monoenergetic electrons through the magnets, we adjusted the different degrees of freedom to achieve good double focusing. Secondly we used a proportional counter and a very small target in order to fix the optimal instrument resolution. This successful method developed for BILL is described in the following sections.

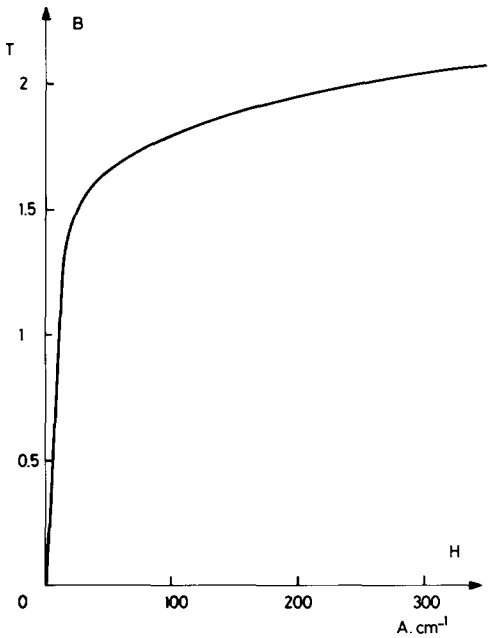

Fig. 7. Magnetization of the iron comprising the magnets of BILL.

3.4.1. *The electron source*

Aiming at an instrumental resolution of 10^{-4}, one has to have a source which delivers monoenergetic electrons with a line width $\Delta p/p$ less than 10^{-4}. Focusing errors can be minimized only if they appear larger than the ideal image of the source. This means that for the second magnet ($D = 540$ cm), a source of 300 keV electrons has to

be smaller than 0.5 mm in diameter and only 100 μg/cm² thick. These dimensions exclude an external radioactive source for an efficient adjustment for reasons of intensity. No intensity problems exist with an internal target in a high flux reactor (even for the photographic method) using the K conversion electrons of the 334 keV transition in ^{150}Sm [6, 7]). The partial cross section of this transition is $\sigma_{part} \approx 1000$ b. A circle, 4 mm in diameter, of natural Sm (14% ^{149}Sm) was evaporated on a 0.2 mg/cm² Al foil. The thickness of the Sm was 0.2 mg/cm². The intensity of the conversion electrons of the 334 keV transition was $I_e = 10^5$/sec at the focal point.

The high electron intensity allowed for a photographic examination of the trajectories not only at the focal point, but also at the cross sections of lowest luminosity. The only disadvantage of a Sm target in a high flux reactor is the short burn up half life ($\sigma = 41\,000$ b) of about 6 hours.

3.4.2. *Detection of the electrons*

The electrons have been detected with X-ray films[6, 7]). Commercial films (Kodirex) are well exposed by 4×10^6 electrons (300 keV) per cm². The exposure time was several seconds in the focal plane and, at most, 30 min at the points of lowest luminosity. The short exposure time compensates by far the disadvantage of the burn-up of the target. The films were mounted into the vacuum tube, enveloped in a light tight plastic foil, for all photographs except those in the focal plane where scattering in the foil would have been too important compared to the small image size.

The procedure for the adjustment was not done in exactly the order described; it was, rather, a semi asymptotic approach by searching for double focusing, aligning the beam, and investigating the influence of the field clamps. Here we report the main stations of the adjustment in the most logical order.

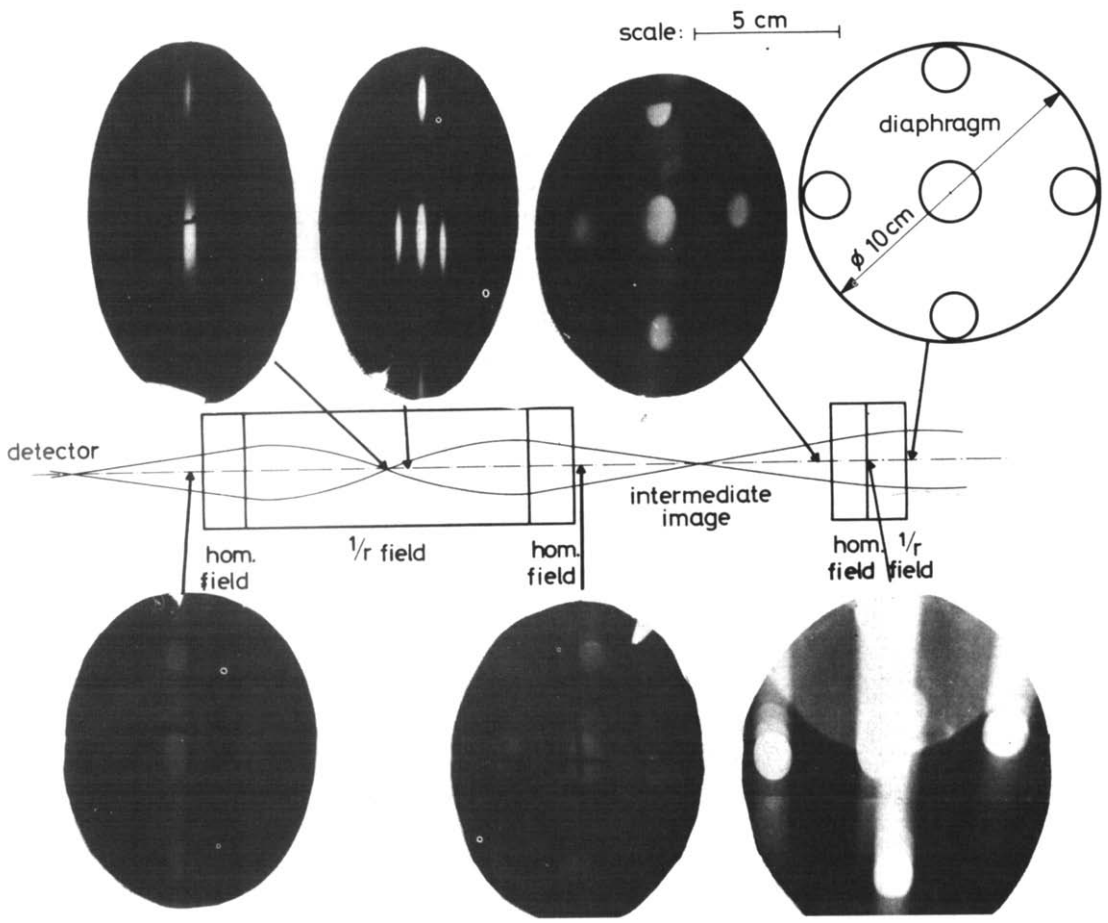

Fig. 8. Five trajectories photographed at different stages in the spectrometer BILL.

3.4.3. *Adjustment of the beam in the vacuum chamber*

Both magnets were installed at the end of the beam tube in such a way that their middle planes were within ± 1 mm of the plane defined by the beam tube and the target changing tube. This adjustment was done with a telescope. The height and the angles between the magnets and the beam have been adjusted to center the beam in the vacuum chamber.

In order to follow simultaneously the central and outer trajectories through the spectrometer a diaphragm with five holes (see fig. 8) was mounted in the beam at the entrance of the first magnet. The study of the outer trajectories allows understanding and correction of focusing errors.

Fig. 8 shows the diaphragm and the size and position of the electron beam (334 keV conversion electrons of ^{150}Sm) through the spectrometer. On the photograph, taken in the first magnet, one can see, in addition, a part of the direct beam and two other conversion electron lines ($E_e = 326.2$ and 392.7 keV). The position of the beam was adjusted to better than 3 mm (beam radius = 100 mm).

3.4.4. *Deflection and focusing of the fringing fields*

Mahlein[4]) suggested limiting the deflection in the fringing fields to 7° by mu-metal tubes of 15 cm diameter (field clamps). Fig. 9 compares the measured and calculated[8]) deflection angles as a function of the distance from the field clamp to the pole piece. Field clamps with a rectangular cross section would correspond better to parallel pole pieces than circular ones which deform the field geometry by a radius dependent cut-off angle. However, rectangular clamps could not be used in our vacuum chamber due to its circular cross section. Therefore, the effective deflection angle is greater than the calculated one for small distances. For large distances the calculation gives deflection angles which are too large due to the idealizing assumption of infinite pole piece width.

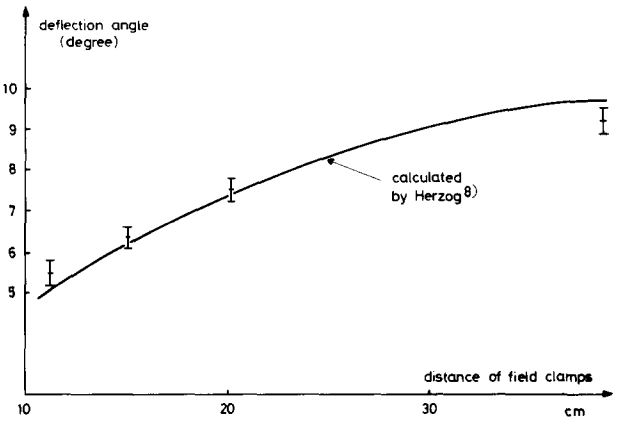

Fig. 9. Measured and calculated deflection angle as a function of the distance of a field clamp with circular cross-section ($r = 15$ cm) from the pole piece.

The fringing fields are not only deflecting but also focusing. Therefore, the distance of the field

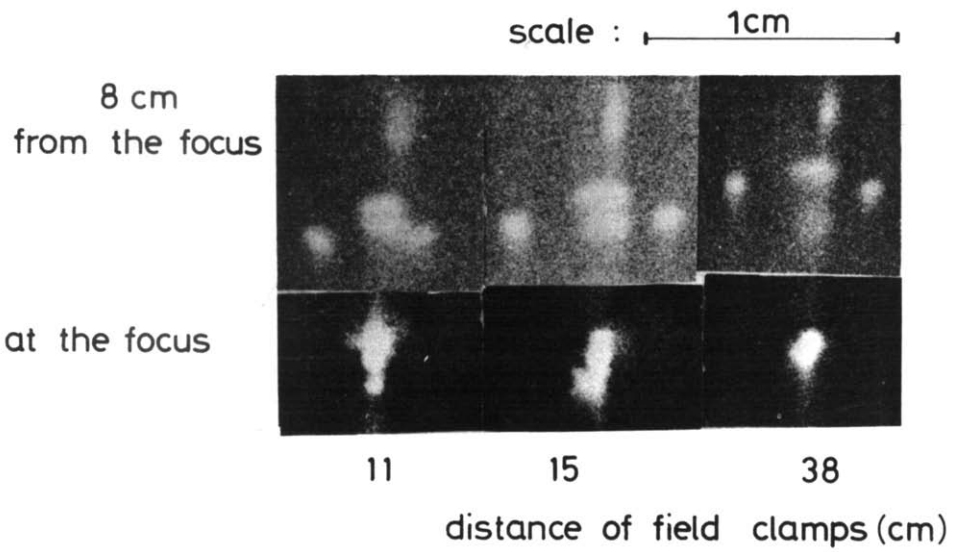

Fig. 10. Quality of the focus as a function of the distance of circular field clamps from the pole piece.

clamps affects the position and the quality of the focus. Fig. 10 shows for three distances of the field clamps the central and the outer trajectory at the focus and at a distance of 8 cm from it. We see clearly that the focusing characteristics deteriorate with smaller distances of the field clamps: the upper and the lower trajectories are not sufficiently deflected and the lateral ones too much. This is due to the radius dependent cut-off of the circular field clamps. Therefore, it was decided to use the largest possible distance of the clamps in order to get best focusing. The maximal distances were either given by reasons of mechanical construction or the necessity to cut off the influence of a neighbouring field.

The final distances (l) and the corresponding deflecting angles are as follows:
- at the entrance of the first magnet: $l = 16$ cm, 6.7°;
- at the exit of the first magnet: $l = 35$ cm, 9.0°;
- at the entrance and exit of the second magnet $l = 25$ cm, 7.3°.

3.4.5. *Double focusing*

Double focusing is obtained by adjusting the angles of the field boundaries with respect to the beam direction. This adjustment is possible by means of the turnable half cylinders in the homogeneous sectors. A larger exit angle ε_2 (see fig. 11), for instance, leads to a larger radial focal length L_{2r} since the inner electrons are deflected more and the outer ones less. On the other hand the axial focal length L_{2z} gets smaller because the axial focusing effect is produced by the oblique crossing of the fringing field. Therefore it is possible to make L_{2r} equal to L_{2z} for one special exit angle ε_2.

From fig. 12 (the adjustment of double focusing of the first magnet), one can directly read the best set of L_2 and ε_2. Focusing errors become very evident in this figure since the ideal image of the target (r = 2 mm) is only about 0.2 mm in diameter.

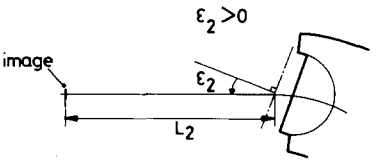

Fig. 11. Definition of the focal length L_2 and the exit angle ε_2.

The results of the adjustment for the two magnets are listed and compared with the calculated values in table 2.

3.4.6. *The focal plane*

The calculation in first order approximation gives no information about a focal plane, therefore an experimental investigation is necessary. Fig. 13 compares two series of photographs (1st magnet). Each film was exposed several times with different fields. The series on the left was taken in the focal plane (57°) and the one on the right in a plane vertical to the beam. The quality of the focus is good over a range of more than 5 cm in the focal plane. The focal plane of the second magnet has an inclination of about 50° in the same sense.

The inclination of the focal plane with respect to the beam allowed for fairly fast adjustment: for one ε_2 one can take several exposures with different fields (corresponding to different L_2) on the same film mounted perpendicularly to the beam. Knowing the angle of the focal plane, one can tell the true focal length L_2 at the center of the focal plane. This method was used for the adjustment shown in fig. 12.

TABLE 2

Calculated and experimental focal length L and angle ε for both magnets after optimum adjustment.

		Distance of object (cm) L_1	Focal length (cm) L_2	Entrance angle ε_1	Exit angle ε_2
M1	calculated	1370	84.7	not variable	− 5°
	measured	1370	88.0		−12°
M2	calculated	87.0	87.0	10°	10°
	measured	94.5	90.4	15°	13°

3.4.7. *Correction of focusing errors*

Focusing errors due to field imperfections remained after the final adjustment. The very sensitive adjustment revealed these errors: the inner and outer trajectories were deflected too much with respect to the central one (see fig. 14a). This effect could only be corrected by curved pole edges. Fig. 15 shows the arrangement of shims which were placed at the edge of the homogeneous sectors to achieve such a curvature. We see

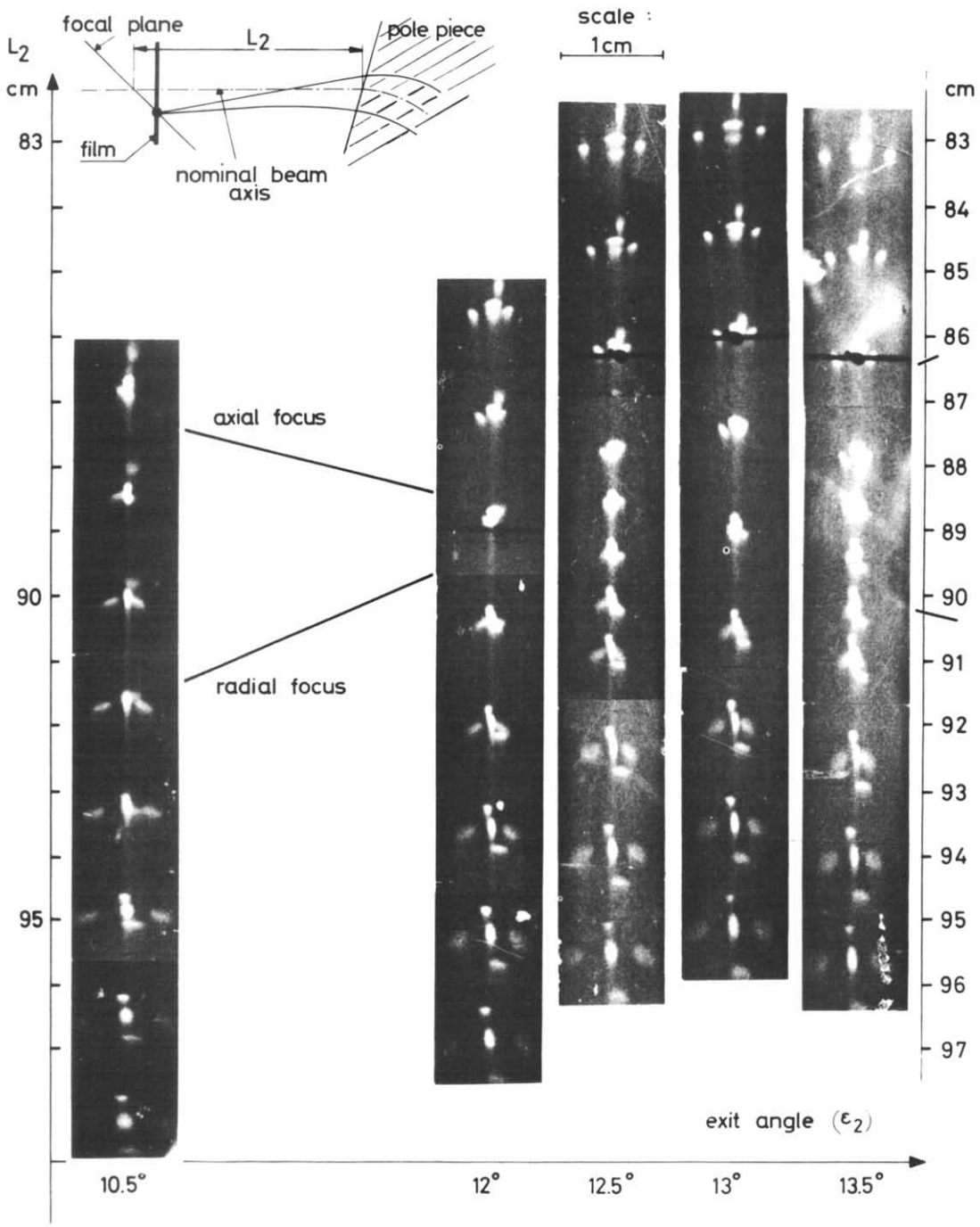

Fig. 12. Adjustment of double focusing for the first magnet by variation of the focal length and the exit angle of the electrons.

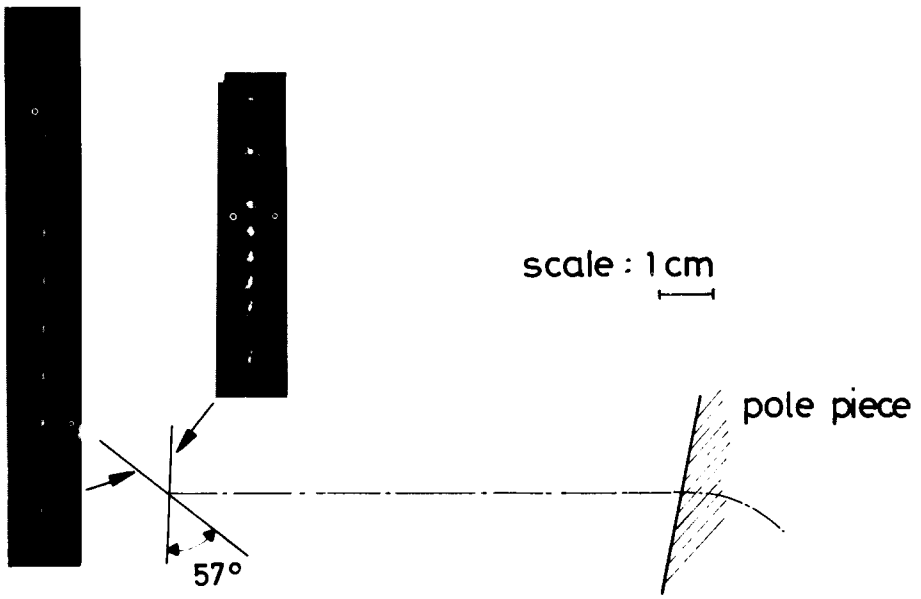

Fig. 13. Demonstration of the focal plane of the first magnet. The photograph at the left was taken at an angle of 57° between a plane vertical to the beam direction and the film. The photograph at the right was taken in the vertical plane.

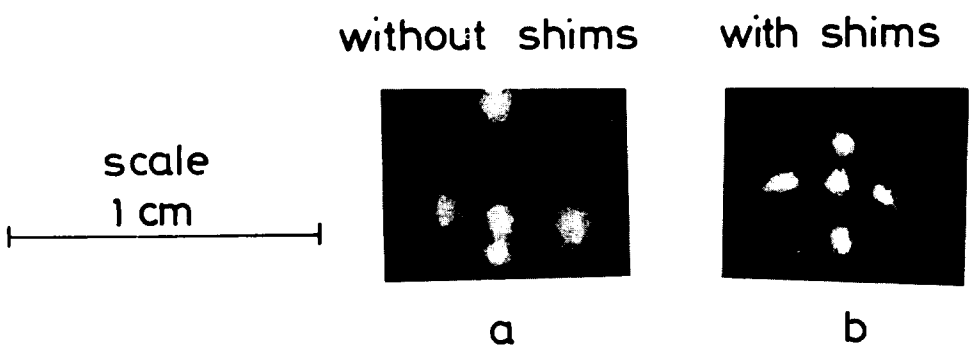

Fig. 14. Effect of shims on the quality of the focus.

the improvement due to these shims in fig. 14b. The effect of the shims is not perfect since their influence on the outer trajectories is stronger than that on the central one (see fig. 14b). To correct this, the pole edges should have been curved over a larger range. However, the remaining errors were very small and therefore the fabrication of complicated ideal shims was unnecessary.

3.5. Stabilization of the magnetic fields

The fields of both magnets are stabilized independently within a precision of better than 10^{-5}. The method of rotating coils[9,10]) is used for this purpose since it provides high precision and linearity for small fields (here $10 < B < 800$ G).

A schematic drawing of the field stabilization circuit is given in fig. 16. Two coils fixed on a common shaft rotate at 33 Hz, one in the magnet-

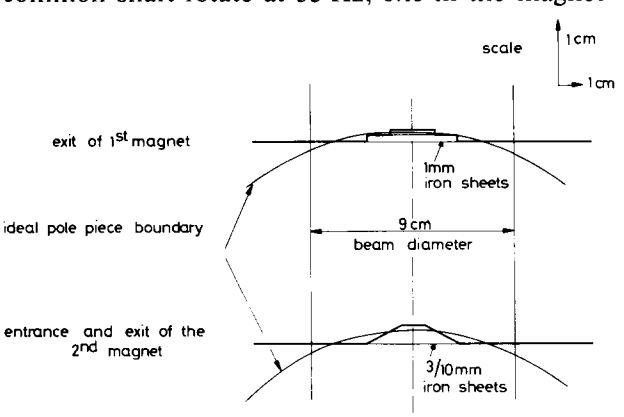

Fig. 15. Form of the shims used for the two magnets.

ic field of the spectrometer, the other in the field of a reference permanent magnet (2000 G) which is temperature stabilized to $\pm 0.1\,^{\circ}C$. The voltage U_0 induced in the reference magnet is divided to αU_0 in an inductive high precision voltage divider with negligible phase shift (ESI, Dekatran DT72A). A comparator delivers the signal $\Delta = \alpha U_0 - U_1$ where U_1 is the voltage induced in the field of the spectrometer magnet. Δ is amplified in a resonance amplifier and demodulated in a phase sensitive rectifier. The resulting dc signal $\bar{\Delta}$ controls the power supply of the magnet such that $\bar{\Delta}$ finally becomes zero. The power supplies are strongly damped (0.01 A/sec for deviations $\Delta B\rho/B\rho < 10^{-4}$ and 0.1 A/sec for deviations $\Delta B\rho/B\rho > 10^{-4}$) in order to avoid overshoots in the stabilization loop.

The technical details of this highly linear and precise magnetic field stabilization will be described elsewhere[11]).

3.6. The demagnetization

Uncontrolled remanences can deteriorate the resolution and change the energy calibration of an iron-core spectrometer. This problem becomes more important with decreasing energy and with increasing resolving power of the instrument. For the spectrometer described, the maximum field of 800 G left an average remanence of 8 G; this is equal to the deflecting field for 15 keV electrons. Therefore the general features of remanences have been studied with much care. In particular, a careful study of possible techniques for an efficient demagnetization were made[12]). Here we will only give a short description of the demagnetization cycle specially adapted for BILL and discuss its results.

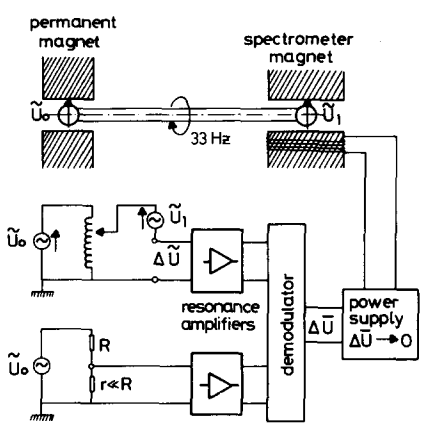

Fig. 16. Schematic drawing of the stabilisation circuit for the magnetic fields.

Ferromagnetic material can be demagnetized by passing through a number of hysteresis loops with decreasing amplitudes. The procedure is defined by

1) the maximal field (current),
2) the amplitude ratio of following loops,
3) the frequency of the loops,
4) the minimal field (current).

Driving the magnetic material into saturation in order to start the demagnetization in a fully reproducible state is not possible. A good compromise between the reproducibility of the remanence and a reasonable power of the demagnetization supply was achieved for the present apparatus, with 3.5 times the maximal measuring current of 40 A.

The amplitude ratio of following loops (a mean value of 0.6) was adjusted experimentally to cancel the remanent field progressively and symmetrically.

The frequency of the loops was the most critical point since eddy currents produce a very inhomogeneous remanent field distribution. Their influence could be kept small in a reasonably fast de-

Table 3

Definition of the demagnetisation cycle for BILL.

Maximal current (A)	Fast region (F) dI/dt (mA/sec)	Slow region (S) amplitude (A)	Slow region (S) dI/dt (mA/sec)
−140			
+140			
−108	500	2	100
+ 69			
− 42	250	1.3	48
+ 25			
− 15.1			
+ 9	100	0.86	48
− 5.4			
+ 3.15	48	0.43	12
− 1.84			
+ 1.08	12	no subdivision	
− 0.64			
+ 0.36			
− 0.22	2,5		

Definition of the cycles 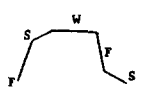

the delay (W) is for all cycles about 1 min

F = fast
S = slow

magnetization by dividing each loop with $I > 3$ A into three parts: a fast one at the beginning followed by a slow one and a wait with $dI/dt = 0$ at the end. The minimal current of the last loop is 220 mA and the current inversion is only allowed for $I < 1$ mA in order to avoid eddy currents.

The complete demagnetization is specified in table 3. It takes 2 h. This demagnetization gave satisfactory results. Recalling that the deflecting field is stabilized by a direct field measurement (see section 3.5), we note that the only remanences which are disturbing are those which do not show the same field distribution as the induced field. The relative difference, $\Delta B_r/B$, of these remanences, integrated over an entire electron trajectory, between the mean trajectory and any other was smaller than 2×10^{-4} after demagnetizing. This value follows from resolution measurements which gave a reproducibility of $\Delta p/p < 2 \times 10^{-4}$ even at 57 keV. At higher energies the relative contribution of the remanences to the total deflecting field is less important and hence the resolution better. The reproducibility of the average field, integrated over the whole beam volume was checked by the shift Δp of a 33 keV line. The line position was measured several times after demagnetizing each time and was found to be reproducible to better than $\Delta p/p = 2 \times 10^{-5}$. This result was even achieved after having driven the field to 800 G (corresponding to 10 MeV) and having demagnetized twice.

3.7. Detectors and response function of BILL

For a beta spectrometer a detector system was desired which had an energy independent sensitivity of 100% for electrons, but a low detection probability for gamma rays. Furthermore, the detector should have a large area (30 mm radial width and 10 mm axial width) and should be position sensitive because of the extended focal plane and the high resolution of BILL. Multiwire proportional counters could fulfill these demands. Two types of detectors, mounted inside the vacuum chamber, were constructed. Both types are operating with a mixture of 90% argon and 10% methane under atmospheric pressure in a flowing mode.

3.7.1. *10 wire detector*

This detector is to be used for electrons with energies between 120 keV and 10 MeV, and is of the Charpak chamber type[13,14]) without separating walls between the ten 2 mm distant wires. The 20 mm long, 20 μm wires of gilded tungsten are placed in a plane between parallel Al foils (1 mg/cm^2) serving as cathodes. The cathodes are at 2100 V and each wire is connected to a charge sensitive amplifier. Since the detector has no entrance slit system, a 1 μsec anticoincidence between each of two neighbouring wires is used to reject the detection of one electron by more than one wire and to reduce the background created by particles not coming from the beam tube. Typical counting rates are 10^5 counts per wire and minute.

The plateau of the detector was measured as a function of high voltage and amplifier gain (with minimally ionizing electrons of 1 MeV). At lower energies the plateau only becomes wider and therefore the entire energy range can be covered remaining at the same detector working point.

In scanning a spectrum using a logarithmic increment, the step width $\Delta p/p$ is chosen such that an integer number of steps lies between two wires, where 1 mm in a plane vertical to the beam corresponds to $\Delta p/p = 1.5 \times 10^{-4}$. The 10 spectra measured by the 10 wires are individually stored as well as added to a sum spectrum after having been shifted with respect to the position of the first wire.

The detector volume is separated from the vacuum by an 800 μg/cm^2 mylar foil. The two windows limit the detector to energies $E > 100$ keV since secondary electrons are scattered to several wires. In addition the limit given by the increasing ionizing power with decreasing energy leads to a wider spread of the secondary electrons. Since multiple detection is rejected the detector becomes energy dependent in sensitivity for energies < 250 keV.

3.7.2. *5 wire detector*

For the reasons described above, a different detector with 5 wires was constructed for energies down to 16 keV as well as for high resolution measurements. This detector has 0.5 mm Al walls between the wires to prevent cross talk and it has a variable entrance slit system. The 4 mm distant wires are at a potential of +1230 V with respect to the walls. The electronics are the same as used for the 10 wire detector. A simple aluminated mylar window (500 μg/cm^2), supported by the entrance slits, serves as cathode and is sufficiently thick to withstand a vacuum. The cut-off energy of this foil is about 12 keV.

3.7.3. *Neutron monitor*

A Li doped glass scintillator was installed to monitor the neutron flux. The statistical error contributed by this monitor is less than 1‰ .

3.7.4. *Response function of BILL*

The response function of the spectrometer (including the detector) does not depend on energy above 150 keV. At low energies the efficiency decreases due to the detector window, but primarily due to disturbing magnetic fields along the 13 m long flight path of the electrons in the beam tube. These disturbing fields are also responsible for the cut-off energy of 16 keV. This response function has been determined using conversion electron lines of ^{116}In [15]) and is shown in fig. 17.

3.8. DATA COLLECTION

The control of the magnetic fields and the data collection is done with a PDP 11. At the beginning of a data run the energy range, the step width, the counting time and the field parameters are entered. The PDP 11 calculates the values of the magnetic fields progressing in logarithmic steps ($\Delta B\rho/B\rho = \text{const.}$) in order to have a constant number of points over a line at all energies. The data are registered on DEC tape.

4. Results

4.1. RESOLUTION AND LINE SHAPE

4.1.1. *Best resolution*

The best resolution and the symmetry of the line shape depend (with an ideal target) primarily on the focusing characteristics of the spectrometer. The best resolution achieved was measured using the L_1 line of the 334 keV transition of ^{150}Sm [16]). The target of natural Sm was 14 μg/cm^2 thick and had an area of 0.2×10 cm^2. A 200 μg/cm^2 Al foil served as backing. The transmission was 8.5×10^{-7} (25% of the total solid angle). The detector slit (0.2 mm) and the target width (0.2 mm) corresponded to $\Delta p/p = 3 \times 10^{-5}$ and 2×10^{-5}, respectively and the natural line width of the L_1 line (6 eV) was equivalent to $\Delta p/p \approx 1 \times 10^{-5}$. Therefore, $\Delta p/p = 7 \times 10^{-5}$ of the measured fwhm (fig. 18) is caused by the instrument resolution (focusing errors). The reasonable symmetry of the line shape indicates that the focusing errors are symmetric for this transmission.

Fig. 19 gives an example of the resolving power as demonstrated by the resolution of the M group of the 334 keV transition measured with the same target.

We can see in fig. 20 how the resolution and line shape depend on the transmission of the spectrometer by using an elliptic diaphragm. The momentum resolution of $\Delta p/p = 1.23 \times 10^{-4}$ is achieved even at full solid angle (3.4×10^{-6}). The asymmetry of the line in this case is due mainly to the asymmetry of the remaining focusing errors which can also be seen in fig. 14 of section 3.4.7.

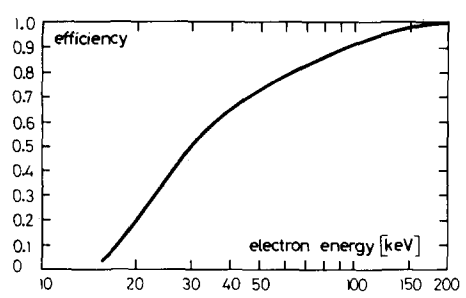

Fig. 17. Response function of the spectrometer BILL (including 5 wire detector). The curve is calibrated to the efficiency = 1 for $E_e > 150$ keV.

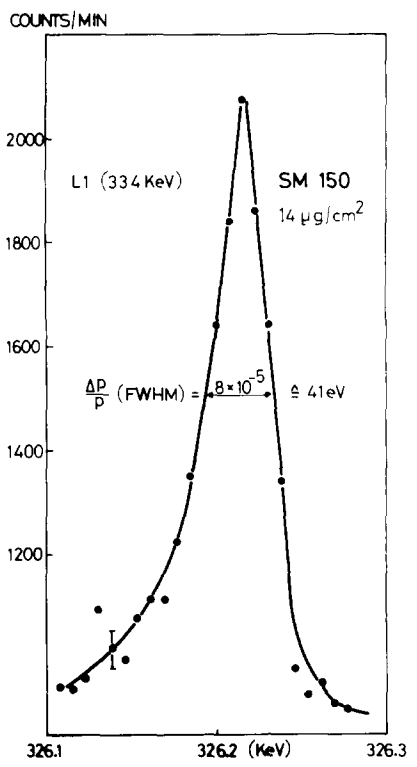

Fig. 18. Best resolution of BILL measured with the L_1 line of the 334 keV transition in ^{150}Sm.

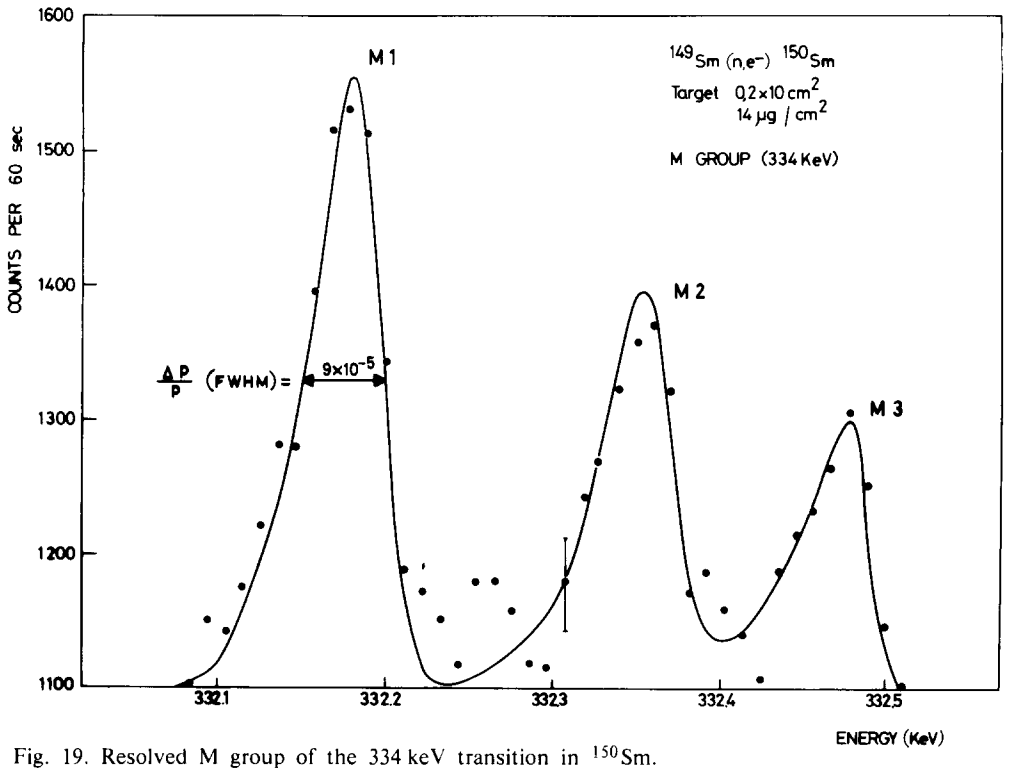

Fig. 19. Resolved M group of the 334 keV transition in ^{150}Sm.

4.1.2. *Energy dependence of the instrument resolution*

The energy dependence of the instrument (intrinsic) resolution was measured with a target of natural indium (15 μg/cm^2, 5×100 mm^2) and full solid angle of the spectrometer. The result is given in fig. 21. The fwhm includes to a smaller extent target thickness effects and natural line width. This energy dependence of the resolution can roughly be explained by a constant defocusing field δB which influences the resolution $\Delta B\rho/B\rho$ mainly at low energies. The major part of δB is due to disturbing magnetic field gradients in the high flux region where no mu-metal tubes could be installed in the beam tube.

4.1.3. *Resolution in routine measurements*

The best resolution was measured with an isotope with very high cross section and with only 25% of the maximal transmission of the instru-

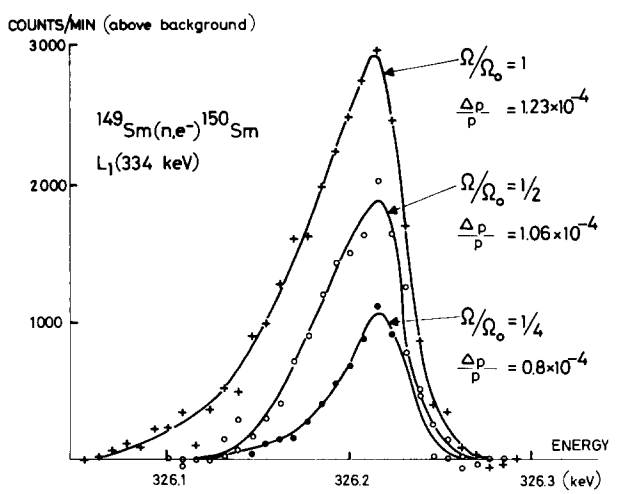

Fig. 20. Momentum resolution of BILL as a function of transmission. Ω_0 is the maximal solid angle of the spectrometer.

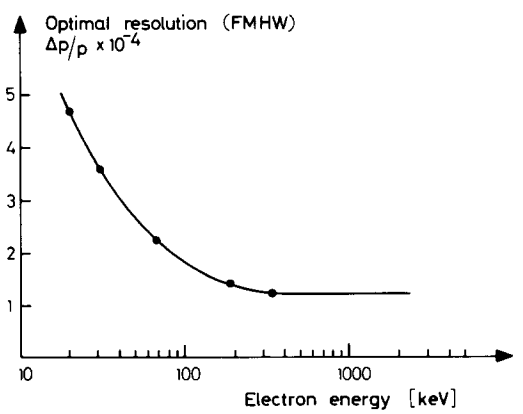

Fig. 21. Measured optimal resolution at full solid angle of BILL as a function of energy.

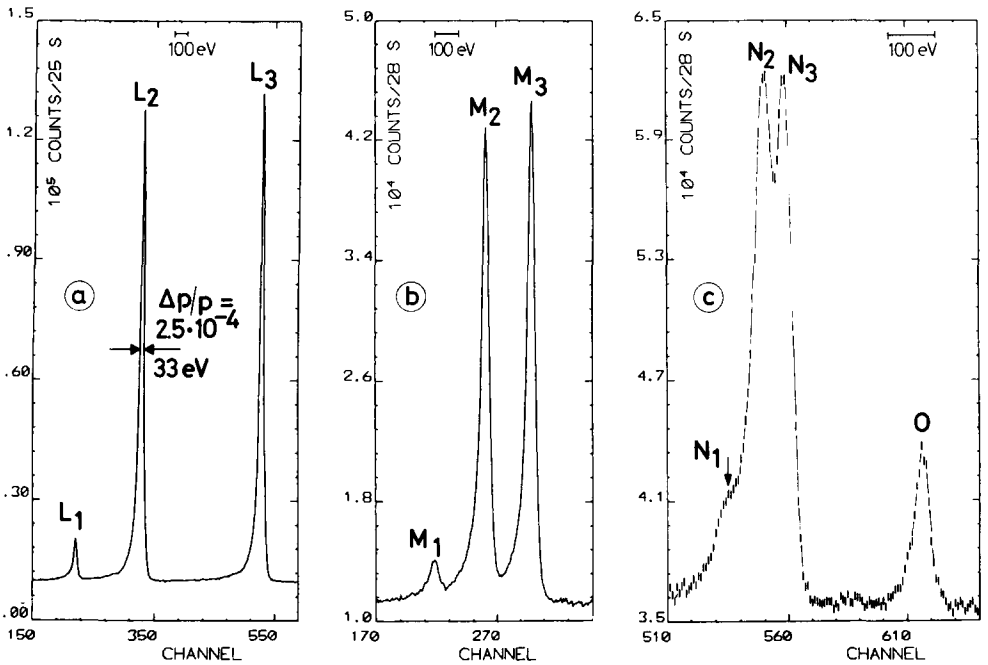

Fig. 22. Subshell groups of the 79.998 keV transition in ^{168}Er. The target was 15 μg/cm^2 thick and had an area of 5×100 mm^2. Note the different energy scales. Plot (c) is a sum spectrum over 3 wires of the multi-wire counter.

tion measurements using maximal transmission and an average cross-section isotope. The measurement in fig. 22 aimed at precise subshell ratios of a pure E2 transition in ^{168}Er. The precision of the relative intensities is better than 1%, and that of the relative energies better than 1 eV. The N and O groups measured in the same high resolution run are also shown.

Routine runs with high sensitivity are done with 30 mm broad targets and 2 mm detector slits. Even then the resolution is about 4×10^{-4} and becomes worse only for thick targets due to the low energy tail. Fig. 23 shows an example for a thin but large target of ^{232}Th, which has a cross section of only 7.4 b for thermal neutrons. The doublets at about 600 keV could clearly be resolved and gave important information on the β-vibration in ^{233}Th [17]). Typical target thicknesses of about 150 μg/cm^2 at 100 keV and up to 5 mg/cm^2 in the MeV region are used for high sensitivity measurements but they cause asymmetric line shapes (see section 4.1.4).

4.1.4. *Line shape with thick targets*

Owing to the very high intrinsic resolution of BILL the line shape in routine runs is determined mainly by the target width and thickness and by ment. We will therefore demonstrate high resolu- the detector slits. The resulting line shape is well fitted by a gaussian form with an exponential tail at the low energy side[18]):

$$y = H\exp[-(x-x_0)^2\,4\ln 2/G^2] + U, \quad \text{for} \quad x \geq x_0,$$

$$y = H\exp[-(x-x_0)^2\,4\ln 2/G^2] +$$

$$+ HS\exp[(x-x_0+GG)\cdot\ln 2/A]\times$$

$$\times\{1-\exp[-(x-x_0)^2\,4\ln 2/GG^2]\} + U,$$

$$\text{for} \quad x < x_0.$$

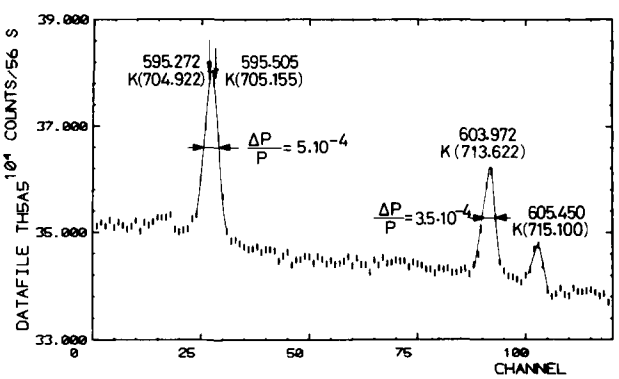

Fig. 23. Example of the investigation of E0 transitions in ^{233}Th [17]). Target: 0.2 mg/cm^2 on 3×10 cm^2.

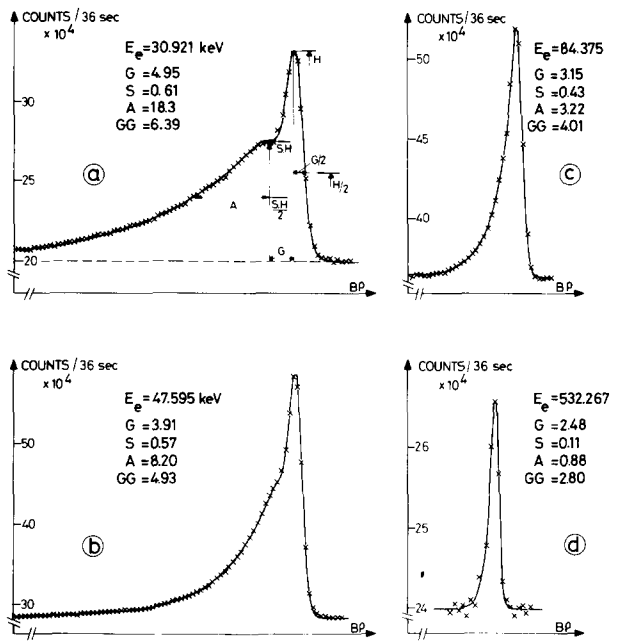

Fig. 24. Demonstration of the quality of the fit function (solid line) for different line shapes corresponding to different energies. The lines are taken from a measurement of ^{121}Sb(n, e)^{122}Sb. A 120 μg/cm^2 layer, 30×100 mm^2, of ^{121}Sb was evaporated on a 200 μg/cm^2 Al backing. The definition and the energy dependence of the fit parameters is shown. All spectra are taken with a step width of $\Delta B\rho/B\rho \mp 1.53\times10^{-4}$.

x_0 is the center of the line and U the background. The four energy dependent shape parameters (G, S, A, GG) are depending on the target width

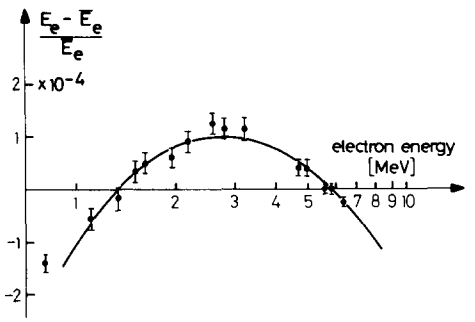

Fig. 25. Measured deviation from linearity between the magnetic field setting (i.e. voltage divider in the field stabilization circuit) and the actual average field seen by the electrons.

and thickness and are fitted for each target using intense, isolated lines at different energies. Fig. 24 shows examples for a ^{122}Sb target (120 μg/cm^2, 30×100 mm^2). We see that the analytic function fits very well even to highly asymmetric lines.

4.2. Energy precision, calibration and reproducibility

Below about 700 keV the statistical (fit) error of stronger electron lines measured with BILL is comparable to that measured with a curved crystal spectrometer (table 4). At higher energies the energy resolution of BILL is even superior to that of a curved crystal spectrometer or a GeLi detector and the energy precision is better.

The actual $B\rho$ values of conversion electron lines should be linearly related to the measured

TABLE 4

Comparison of transition energies in ^{122}Sb [24]) obtained from measurements with the curved crystal spectrometer GAMS 1 and BILL.

E_γ [1]) (keV)	ΔE_γ (eV)	shell	$E_\gamma - E_B$ [2]) (keV)	E_e [3]) (keV)	$(\Delta E_e)_{stat.}$ [4]) (eV)	$(\Delta E_e)_{tot}$ [5]) (eV)	δE [6]) (eV)
61.4110	0.4	K	30.9200	30.9210	0.4	0.7	−1.0
71.4648	0.8	K	40.9738	40.9726	0.7	0.8	+1.2
78.0885	1.0	K	47.5975	47.5945	0.3	0.6	+3.0
88.2666	1.0	K	57.7756	57.7779	0.4	0.8	−2.3
71.4648	0.8	L1	66.7668	66.7679	1.5	1.6	−1.0
105.8139	1.5	K	75.3229	75.3225	0.4	1.1	+0.4
114.8660	2.0	K	84.3750	84.3750	0.3	1.2	0.0
124.0260	1.0	K	93.5350	93.5357	1.7	2.3	−0.8

[1]) E_γ taken from the (n, γ) measurement at the curved crystal spectrometer GAMS 1 [24]).
[2]) Electron binding energy E_B from ref. 1.
[3]) Results from a weighted least square fit to a straight line between the $B\rho$ value measured at BILL and the $B\rho$ value deduced from E_γ. χ^2 of the fit: 1.24.
[4]) Fit error of the electron lines.
[5]) Total error, including calibration to the γ-lines.
[6]) $\delta E = (E_\gamma - E_B) - E_e$.

$B\rho$ values deduced from the setting of the voltage divider in the regulation circuit of the magnetic field (see section 3.5). This linearity may be disturbed for higher fields by saturation effects at the pole edges and in the mu-metal field clamps.

At lower energies the linearity can be checked by comparing results from curved crystal spectrometers with those of BILL. As shown in table 4 a fit of a straight line between the measured $B\rho$ values and $B\rho$ deduced from E_γ measurements is possible over a considerably wide energy range, even if the line shape changes drastically (see fig. 24 from the same measurement). Small deviations from the linearity over a wider energy range at lower energies in the order of some 10^{-5} may be due to disturbing external magnetic fields but cannot be distinguished from line shape effects.

The linearity at higher energies can only be checked indirectly. Combinations of precisely known low energy transitions with their high energy crossovers can be used for this purpose. For our linearity test levels in ^{200}Hg were used[19]). The result is given in fig. 25. The magnitude of the deviation from linearity is of the order which is expected for the mentioned saturation effects. One can well describe this curve between 800 keV and 7 MeV by a second order term, which has been proved by several measurements to be a constant of the spectrometer within 10^{-5}. Due to this precision Q-values of the n-capture process and energies of primary transitions were measured with a precision of 10^{-5} [20]).

The energy reproducibility is better than 2×10^{-5} as already discussed in section 3.6.

4.3. Background, sensitivity and intensity precision

Two collimators prevent those electrons generated in the beam tube from directly reaching the spectrometer (see section 3.2) where they might contribute to the background. However, three main contributions remain:

1) electrons from the bottom of the beam tube;
2) electrons scattered or generated by gamma rays at the target;
3) electrons scattered or generated by gamma rays at the collimator edges.

The background as a function of energy has been measured (fig. 26) for the empty beam tube, with the source holder and with different targets. The Al-backing foil (see section 3.2) contributes mainly at lower energies. One can clearly see the cut-off by the beam tube at about 16 keV and the strong decrease of the background for $E>5$ MeV.

The sensitivity of the instrument is determined by the neutron flux, the solid angle, the beam tube and detector response function and by the background. These components have been dis-

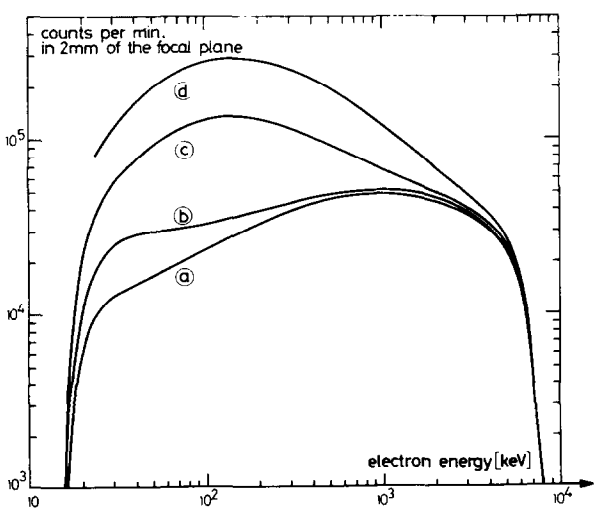

Fig. 26. Background of the spectrometer BILL measured in the focal plane of the second magnet. (a) empty beam tube. (b) with target holder. (c) with a 150 μg/cm^2 Pd target (30×100 mm^2) on 200 μg/cm^2 Al backing. (d) with 150 μg/cm^2 Cm (20×100 mm^2) on 2 mg/cm^2 Ni backing.

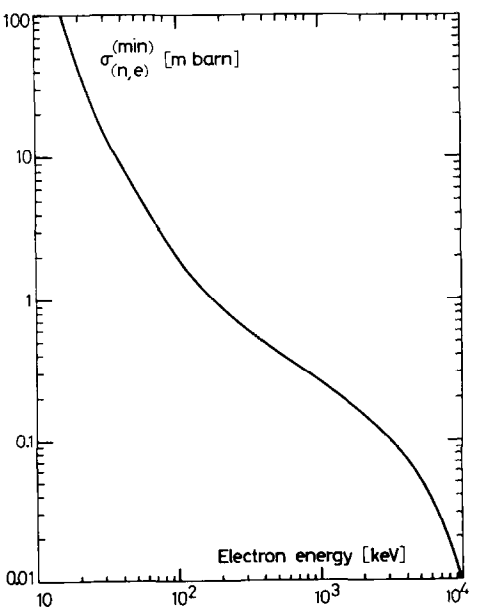

Fig. 27. Sensitivity function of BILL. The minimal partial cross-section for the (n, e) reaction is given. A line is accepted if its height exceeds $3\times$(background)$^{1/2}$ measuring 1 min per point.

cussed separately. Fig. 27 shows the measured sensitivity, defined as the minimum measured partial cross section for the (n, e) reaction, as a function of energy. The target thickness and the detector have to be matched to the energy region.

In cases of special interest the sensitivity can be increased by scanning several times over the region of interest. Fig. 28 shows an example of such a measurement, which took 38 h. No loss of resolution is visible, which proves the high stability of the instrument.

Within a period of a routine run (about 14 d) the relative intensities are reproducible to about 1%. Relative intensities of strong neighbouring lines however can be measured with a precision of a few parts in 10^3. Since the response function of the instrument is very well known and constant for $E_e > 150$ keV, the spectrometer is frequently used to calibrate γ-spectra using well-known transitions and reliably calculated internal conversion coefficients.

5. Conclusion

The electron spectrometer BILL has been in continuous operation since 1975. It has surpassed many of the design criteria discussed in section 2. The very high sensitivity is due to the relatively low background, the application of multiwire detectors and mainly to the high neutron flux of the HFR in Grenoble. The large target area (up to 40 cm^2) leads to a high luminosity in spite of the solid angle of 3.4×10^{-6}. The resolution of 8×10^{-5} in momentum is the best achieved up to now with a beta spectrometer. To obtain this resolution the transmission was reduced only by a factor of four. This resolution was obtained by the very large dispersion of the magnets, by sufficient degrees of freedom to correct the focusing properties, and by a very careful demagnetization procedure. This result shows that iron core spectrometers are well suited to very high resolution measurements. The optimum resolution might be improved by better field shims, better mu-metal field shields and an additional field correction in the intermediate axial focus of the second magnet. However, in practical cases, the natural line width and the target thickness are severe limitations on the resolution. Moreover, the standard resolution of 4×10^{-4} is sufficient for most measurements. The momentum precision is of the order of 10^{-5} and, therefore, at low energies ($E < 700$ keV) comparable to curved crystal gamma ray measurements and at high energies superior to GeLi measurements.

The experiments performed so far with BILL are listed in table 5. The experiments concern nuclear spectroscopy and precision measurements of conversion coefficients, energies and natural line widths. Neutron binding energies have been determined with a precision of better than 100 eV. The success in nuclear spectroscopy depends to a large extent on the combination with the results of the crystal spectrometers[38]) and the pair and anti-Compton spectrometers installed at the ILL. For example, the conversion coefficients measured with BILL allowed the identification of E0 components in transitions in odd actinide isotopes[17,33,34]). These transitions together with strong E2 and E1 transitions helped to establish in actinide nuclei many vibrational structures which are very difficult to detect with other spectroscopic methods.

According to the structure of the Institut Laue–Langevin, all interested physicists can sub-

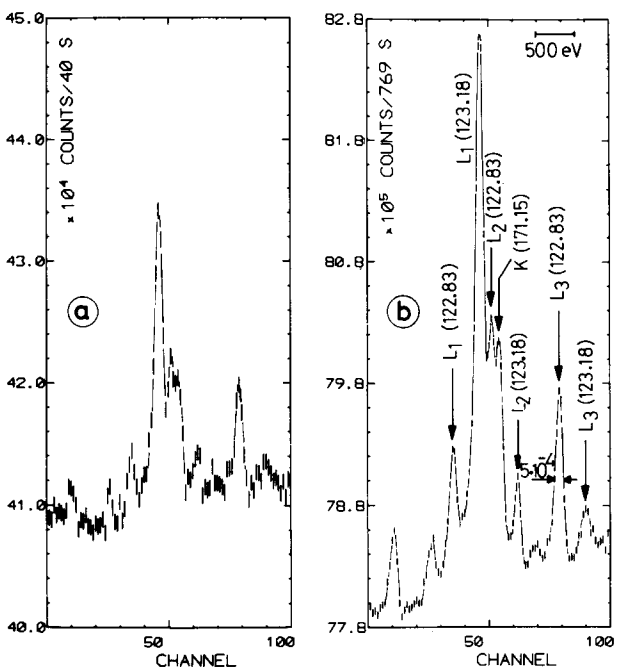

Fig. 28. Example of the gain in sensitivity obtained by multi-scanning a region of particular interest. (a) shows a single scan and (b) the sum over 19 scans. The total measuring time was 38 h. No change in resolution due to summing was observed. The target isotope was ^{167}Er, 80 μg/cm^2 on 30×100 mm^2. The L_1/L_3 ratio of the 122.83 keV, $5^+ \rightarrow 4^+$ transition in the 2^+ γ-band of ^{168}Er could be determined with an error of only 5%.

TABLE 5
Experiments performed with BILL.

Final nucleus	Proposer	Laboratory	Reference
nuclear spectroscopy			
^{80}Br, ^{82}Br	H. P. Do et al.	Lyon, France	21
^{100}Tc	J. A. Pinston et al.	ILL	22
^{109}Pd	R. F. Casten et al.	Brookhaven, U.S.A.	23
^{122}Sb, ^{124}Sb	V. L. Alexeev et al.	Leningrad, U.S.S.R.	24
^{147}Nd	R. Roussille et al.	ILL	25
^{149}Nd	K. Schreckenbach	ILL	26
^{151}Nd	J. A. Pinston et al.	ILL	27
^{155}Sm	R. K. Smither et al.	Argonne, U.S.A.	28
^{154}Eu, ^{155}Eu, ^{156}Eu	P. T. Prokofiev et al.	Riga, U.S.S.R.	29
^{155}Gd	W. Stöffl et al.	Munich, Germany	30
^{168}Er	W. Gelletly et al.	Manchester, U.K.	31
^{172}Yb, ^{174}Yb	J. Larysz et al.	ILL	32
^{190}Os	R. F. Casten et al.	Brookhaven, U.S.A.	23
^{196}Pt	R. F. Casten et al.	Brookhaven, U.S.A.	23
^{231}Th	D. H. White et al.	Oregon, U.S.A.	39
^{233}Th	P. Jeuch et al.	ILL	17
^{235}U	J. Almeida et al.	ISN, Grenoble, France	33
^{239}U	H. G. Börner et al.	Jülich, Germany	34
^{238}Np	J. Kern et al.	Fribourg, Switzerland	40
^{249}Cm	R. W. Hoff et al.	Livermore, U.S.A.	35
conversion coefficients, precise energies, natural line widths			
^{56}Mn, ^{116}In, ^{198}Au	K. Schreckenbach	ILL	26
^{92}Zr, ^{114}Cd, ^{165}Dy, ^{200}Hg	F. Braumandl et al.	ILL	20
^{152}Eu, ^{154}Eu	G. M. Kalvius et al.	Munich, Germany	36
^{162}Dy, ^{164}Dy, ^{168}Er	W. Gelletly et al.	Manchester, U.K.	37

mit proposals for experiments with BILL and cooperation with other institutes is welcomed, as can be seen from table 5.

The authors wish to thank Prof. H. Maier-Leibnitz who initiated this work and gave encouraging support. The essential support of Prof. R. Mössbauer is gratefully acknowledged. We are indebted to Drs. H. G. Börner, W. F. Davidson, D. Heck, H. R. Koch, J. A. Pinston and D. D. Warner of the (n, γ) group of the I.L.L. for their amicable cooperation. We are grateful for important technical help from G. Blanc, who is presently the technician responsible for BILL, G. Edenhofer, J. C. Faudou, J. P. Giraud, G. Schuba and K. Ben Saidane. The excellent cooperation of the reactor and technical staff of the I.L.L. is very much appreciated.

References

1) K. Siegbahn, *Alpha- beta and gamma-ray spectroscopy*, vol. 1 (ed. K. Siegbahn; North-Holland, Amsterdam, 1965) p. 79, and H. Motz and G. Bäckström, ibid., p. 769.
2) T. von Egidy, Nucl. Data Tables **A7** (1970) 465.
3) T. von Egidy, Ann. Physik **9** (1962) 221.
4) H. F. Mahlein, Nucl. Instr. and Meth. **53** (1967) 229.
5) J. C. Faudou and B. P. K. Maier, Kerntechnik **11** (1974) 496.
6) E. Bieber, Z. Physik **189** (1966) 217.
7) W. Mampe, Ph. D. Thesis, T. U. München (1971).
8) R. F. K. Herzog, Z. Naturf. **10a** (1955) 887.
9) G. Bäckström. Nucl. Instr. and Meth. **1** (1957) 253.
10) W. Nörenberg, Z. angew. Physik **17** (1964) 452.
11) K. Schreckenbach, to be published.
12) P. Jeuch and W. Mampe, Nucl. Instr. and Meth. **140** (1977) 347.
13) G. Charpak, R. Bouclier, T. Bressani, J. Favier, C. Zupancic, Nucl. Instr. and Meth. **62** (1968) 235.
14) B. Olma, Ph. D. Thesis, T.U. München (1973).
15) K. Schreckenbach, A. A. Suarez and T. von Egidy, Z. Naturf. **28a** (1973) 1308.
16) W. Mampe, P. Jeuch, T. von Egidy, K. Schreckenbach, F. Braumandl and J. Larysz, Nucl. Instr. and Meth. **128** (1975) 585.
17) P. Jeuch, K. Schreckenbach, F. Braumandl, T. von Egidy, J. Larysz and W. Mampe, Proc. Int. Conf. Lowell, Mass., U.S.A. (1976), and to be published.
18) T. von Egidy, Habilitationsschrift, T.U. München (1968).

[19]) D. Breitig, R. F. Casten and G. W. Cole, Phys. Rev. **C9** (1974) 366.
[20]) F. Braumandl, Ph. D. Thesis, T.U. München (1978).
[21]) H. P. Do, R. Chery, H. Börner, W. F. Davidson, J. A. Pinston, R. Roussille, K. Schreckenbach, H. R. Koch, H. Seyfarth and D. Heck, Z. Physik **286** (1978) 107.
[22]) J. A. Pinston, D. Heck, H. R. Koch, H. G. Börner, R. Roussille, W. Mampe, P. Jeuch and K. Schreckenbach, to be published.
[23]) R. F. Casten, W. F. Davidson, J. A. Pinston, K. Schreckenbach and D. D. Warner, to be published.
[24]) V. L. Alexeev, B. A. Emelianov, A. I. Egorov, L. P. Kabina, D. M. Kaminker, Yu. L. Khazov, I. A. Kondurov, E. K. Lenshkin, Yu. E. Loginov, V. V. Martynov, V. L. Rumiantsev, S. L. Sakharov, P. A. Sushkov, H. G. Börner, W. F. Davidson, J. A. Pinston and K. Schreckenbach, Nucl. Phys. **A297** (1978) 373.
[25]) R. Roussille, J. A. Pinston, H. Börner and H. R. Koch, Nucl. Phys. **A246** (1975) 380.
[26]) K. Schreckenbach, to be published.
[27]) J. A. Pinston, R. Roussille, H. Börner, W. F. Davidson, P. Jeuch, H. R. Koch and K. Schreckenbach, Nucl. Phys. **A270** (1976) 61.
[28]) R. K. Smither, K. Schreckenbach, A. I. Namenson, W. F. Davidson, H. G. Börner, J. A. Pinston, D. D. Warner and T. von Egidy, Proc. Int. Conf. *Nucl. Structure*, Contr. Papers, Tokyo (September 1977); published by Organizing Committee, Tokyo (1977) p. 393.
[29]) P. T. Prokofiev, M. K. Balodis, A. J. Krumina, N. D. Kramer, M. N. Plate, L. I. Simonova, K. Schreckenbach, W. F. Davidson, J. A. Pinston, D. D. Warner, H. G. Börner and P. H. M. van Assche, Proc. Conf. *Nucl. Structure*, Contr. Papers, Tokyo (Sept. 1977); publ. by Organizing Committee, Tokyo (1977) p. 390, 394.
[30]) W. Stöffl, K. Schreckenbach, H. G. Börner, W. F. Davidson, D. D. Warner and T. von Egidy, to be published.
[31]) W. Gelletly, W. F. Davidson, J. Simic, K. Schreckenbach, H. G. Börner and D. D. Warner, to be published.
[32]) J. Larysz, W. Gelletly, K. Schreckenbach, W. Mampe, H. G. Börner, W. F. Davidson, J. A. Pinston and D. D. Warner, to be published.
[33]) J. Almeida, H. G. Börner, W. F. Davidson, K. Schreckenbach, A. I. Namenson, T. von Egidy and P. H. M. van Assche, Proc. Int. Conf. *Nucl. Structure*, Contr. Papers, Tokyo (Sept. 1977); publ. by Organizing Committee, Tokyo (1977) p. 463, and to be published.
[34]) H. G. Börner, H. R. Koch, H. Seyfarth, T. von Egidy, W. Mampe, J. A. Pinston, K. Schreckenbach and D. Heck, Z. Physik **A286** (1978) 31.
[35]) R. W. Hoff, W. F. Davidson, D. D. Warner, K. Schreckenbach, H. Börner, A. F. Diggory and T. von Egidy, Proc. Int. Conf. *Nucl. Structure*, Contr. Papers, Tokyo (Sept. 1977); publ. by Organizing Committee, Tokyo (1977) p. 465.
[36]) G. M. Kalvius and K. Schreckenbach, to be published.
[37]) W. Gelletly and K. Schreckenbach, to be published.
[38]) H. Börner, P. Göttel, H. R. Koch, J. Pinston and R. Roussille, Proc. 2nd Int. Symp. on *Neutron capture gamma ray spectroscopy and related topics*, Petten, the Netherlands (1974) p. 697.
[39]) D. H. White and R. W. Hoff et al., to be published.
[40]) J. Kern et al., to be published.